ChemComm

COMMUNICATION

View Article Online
View Journal | View Issue

Cite this: *Chem. Commun.*, 2016, 52, 104

Received 22nd September 2015,
Accepted 15th October 2015

DOI: 10.1039/c5cc07936e

www.rsc.org/chemcomm

Published on 15 October 2015. Downloaded on 19/05/2017 11:54:47.

# Nickel as a co-catalyst for photocatalytic hydrogen evolution on graphitic-carbon nitride (sg-CN): what is the nature of the active species?†

Arindam Indra,[a] Prashanth W. Menezes,[a] Kamalakannan Kailasam,[b] Dirk Hollmann,[c] Marc Schröder,[a] Arne Thomas,[a] Angelika Brückner[c] and Matthias Driess*[a]

**The nature of a nickel-based co-catalyst deposited on a sol–gel prepared porous graphitic-carbon nitride (sg-CN), for photocatalytic $H_2$ production from water, has been investigated. The formation of the active catalytic species, charge separation and recombination of the photogenerated electrons and holes during photochemical $H_2$ evolution has been determined for the first time using *in situ* EPR spectroscopy.**

The use of solar light for photocatalytic water-splitting into dihydrogen ($H_2$) and dioxygen ($O_2$) with semiconductor catalysts has been considered to be a sustainable way of energy production, as an alternative to using the steadily decreasing and environmentally pollutant fossil fuels.[1,2] For effective harvesting of visible light, the semiconductor must have a band gap higher than 1.23 eV and the conduction band must be more negative than the reduction potential of $H^+/H_2$.[3] Moreover, the separation of the photogenerated electrons and holes competing with their recombination is an additional challenge in photocatalytic water-splitting.[4]

Noble metals, such as Pt for the hydrogen evolution reaction (HER), have been of increasing interest in recent years and widely applied as co-catalysts to hasten the electron transport pathway.[5,6] The decorated nanoparticles of noble metals on a catalyst surface act as electron sinks to supply charge separation across the interface or heterojunction. Lately, several CdX (X = S, Se)-based photocatalytic systems have been studied to understand the lifetime of the photogenerated electrons and holes, and their recombination during photocatalytic HER.[7] Interestingly, the organic carbon nitride photocatalyst has been effective for hydrogen evolution under visible light irradiation[8] whereas, a Pt-containing graphitic carbon nitride (g-CN) system has been investigated to uncover the charge separation and recombination phenomena.[9] Several efficient systems with a combination of Pt and g-CN have been examined for enhanced HER,[10–14] but a Pt-free approach to give similarly active catalysts remains of particular interest. In the last few years, the Pt- free approach has been demonstrated for HER by combining g-CNs with $MoS_2$,[15] CdS,[16] $CuInS_2$,[17] NiS,[18] $Ni(OH)_2$,[19] ZnO[20] with low to moderate activity. In addition, Ag or Au nanoparticles deposited on g-CN nanocomposites were also studied to achieve plasmonic enhancement in the photocatalytic activity.[21,22] Interestingly, the combination of molecular metal complexes with g-CN have been probed for photocatalytic HER as well, however, leading to the attainment of less active photocatalysts than the Pt–g-CN systems.[23]

The development of $H_2$ evolution catalysts that combine g-CN with cheap and abundant metals, such as Ni as a co-catalyst, is highly desired for effective and stable hydrogen production.[24] Although Ni-based catalyst systems have been explored in recent years,[24,25] to our knowledge, no attempt has been reported to uncover the nature and structural features of the Ni co-catalyst as well as the possible structural and bonding situation occurring at the co-catalyst active sites during photocatalytic HER. In line with that, the separation and recombination processes of the photogenerated electrons and holes with the Ni–CN system have not been perceived so far. Encouraged by our recent results on the determination of the active sites of oxygen evolution catalysts,[26–28] we directed ourselves toward model catalytic systems by depositing non-noble metal co-catalysts to elucidate the role of the co-catalyst during photocatalytic HER.

For this purpose, we have chosen photocatalytically highly active porous sol–gel prepared g-CN[6] (abbreviated as sg-CN hereafter) with a photodeposited nickel species as the co-catalyst to achieve long-term HER in the presence of the sacrificial electron donor (SD) triethanolamine (TEOA). After photodeposition, the materials were extensively characterized using various spectroscopic, microscopic and analytical tools. The structural changes of the Ni co-catalyst were thoroughly studied during photocatalytic

[a] *Metalorganic Chemistry and Inorganic Materials, Department of Chemistry, Technische Universität Berlin, Strasse des 17 Juni 135, Sekr. C2, D-10623 Berlin, Germany. E-mail: matthias.driess@tu-berlin.de*
[b] *Institute of Nano Science and Technology, Mohali, Punjab 160062, India*
[c] *Leibniz Institute for Catalysis at the University of Rostock, Albert Einstein-Straße 29A, 18059 Rostock, Germany*

† Electronic supplementary information (ESI) available: Complete experimental details and characterization of Ni–CN catalysts before and after photochemical hydrogen evolution. See DOI: 10.1039/c5cc07936e


This journal is © The Royal Society of Chemistry 2016

Published on 15 October 2015. Downloaded on 19/05/2017 11:54:47.

HER using *in situ* electron paramagnetic resonance (EPR) and the recovered samples were also subsequently studied by EPR, X-ray photoelectron spectroscopy (XPS), and high resolution transmission electron microscopy (HR-TEM) to uncover the complete structural situation.

First of all, the co-catalyst has been loaded onto sg-CN using a $Ni^{2+}$ salts under different reaction conditions (Table S1 and the Experimental section in the ESI†). The following abbreviations are used for the prepared samples: Cat-1 (photodeposition, with SD), Cat-2 (deposition in the dark, with SD), Cat-3 (photodeposition, without SD). It is worth mentioning here that the presence of both light and TEOA is necessary for the efficient deposition of $Ni^0$ nanoparticles for enhancing the catalytic hydrogen evolution (see later). TEOA accepts the photogenerated holes and helps in the reduction of $Ni^{2+}$ to $Ni^0$ whereas in the absence of light, no photoexcitation occurs and only a small amount of the nickel species is deposited on sg-CN.

An extensive characterization of the materials has been performed to understand the structural features of the catalyst and oxidation state of nickel, and its binding interaction with sg-CN. Powder X-ray diffraction (PXRD) of Cat-1 showed two peaks at $2\theta$ values of 13° and 27.4° which correspond to the typical intra-planar arrangement in a sheet and graphitic stacking peak (Fig. S1, ESI†). No new peak was detected after the loading of nickel species onto g-CN under different deposition conditions (Fig. S1, ESI†). The loading of Ni was confirmed by energy dispersive X-ray spectroscopy (EDX, Fig. S2, ESI†) and inductively coupled plasma atomic emission spectroscopy (ICP-AES, Table S1, ESI†). The latter revealed a nickel content of 0.73 wt% in Cat-1 when photodeposition was performed in the presence of SD. However, in the absence of SD or light, a lower loading of nickel (0.1 wt%) was found.

For all catalysts, the ratio of N to C was determined to be ~1.3 by elemental analyses. The $^{13}C$ cross-polarization/magic angle spinning solid state (CP/MAS) NMR spectrum of Cat-1 showed a heptazine-based structure of the sg-CN with the $CN_3$ moiety resonating at $\delta$ 154 ppm and the $C(N)_2(NH)_x$ moiety at 162 ppm, respectively. No shift of these peaks was observed after the deposition of the nickel species on this sg-CN material (Fig. S3, ESI†). In addition, the BET (Brunauer–Emmett–Teller) surface area of sg-CN (147 $m^2\ g^{-1}$), after photodeposition in Cat-1 (142 $m^2\ g^{-1}$), was merely changed. In the UV-Vis spectra, the maximum absorption for Cat-1 was observed at $\nu$ = 360 nm but for other catalysts, significant variations in the band positions were found that were reflected in their catalytic activities (Fig. S4a, ESI†). Infrared spectroscopy (IR) confirmed the unchanged sg-CN structure (Fig. S4b, ESI†). TEM and HRTEM measurements displayed the porous structure of sg-CN without any discrete crystallites corresponding to $Ni^0$, NiO or NiOOH in Cat-1 (Fig. S5, ESI†).

What is the nature of the deposited Ni-species as co-catalyst? At first we determined the oxidation state of nickel in Cat-1 after photodeposition. On the surface of the catalyst only a very low amount of nickel could be detected by XPS. The $Ni2p_{3/2}$ peak at binding energy of 856.8 eV suggests an oxidation state +2. Furthermore, the presence of metallic nickel is indicated by the peak at 853 eV in Cat-1 (Fig. S6a, ESI†).[29] It should be mentioned here that in Cat-1, the amount of nickel at the outer surface was relatively low and most of the nickel was present in the bulk of the porous sg-CN (total 0.73%). The N1s XPS peak could be deconvoluted into two peaks corresponding to N-pyridine moieties at 399.8 eV and graphitic C═N subunits at 401.7 eV, respectively (Fig. S6b, ESI†).[30] The C1s XPS peaks could be attributed to C═C, C═N and C–N moieties from lower to higher energy (Fig. S6c, ESI†), while the O1s spectrum of Cat-1 represents surface adsorbed oxygen species and C–O bonds (Fig. S6d, ESI†).[30]

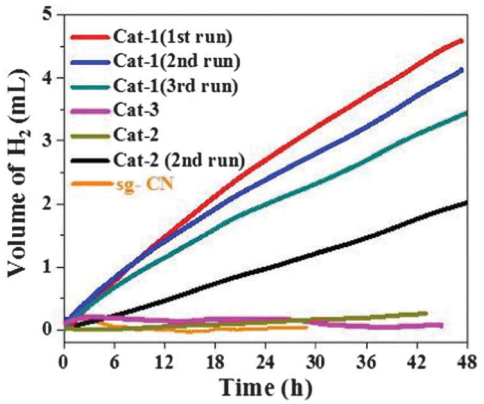


Fig. 1 Photocatalytic $H_2$ evolution profiles of various catalysts in the presence of 300 W Xe lamp with a cut off filter of 420 nm using TEOA as the sacrificial agent.

After the initial characterization of the two components of the catalysts (photocatalyst and co-catalysts), we further investigated the catalysts for the photochemical $H_2$ evolution (Fig. 1). Under visible light irradiation (>420 nm), the highest amount of $H_2$ evolution was observed with Cat-1 whereas the other catalysts showed much less activity. Under similar reaction conditions, negligible amount of $H_2$ production could be detected with co-catalyst-free sg-CN. The rate of $H_2$ evolution for Cat-1 was calculated at 0.103 $mmol_{H_2}\ g_{cat}^{-1}\ h^{-1}$ in the first 4 h for Cat-1. The rate of $H_2$ production for Cat-1 is comparable with related CN-based materials loaded with non-noble metal-containing co-catalysts.[31] For example, previously NiS–g-CN has shown a $H_2$ evolution rate of ~0.4 $mmol_{H_2}\ g_{cat}^{-1}\ h^{-1}$.[18] The photocatalyst Cat-1 was recycled three times to yield a total of 12.2 mL of $H_2$ (Fig. 1) after ~128 h. A turnover number (TON = mol of $H_2$ produced per mol of Ni) of 79 was achieved in terms of the total amount of loaded nickel. A minor loss of activity, after three cycles was observed in Cat-1 and long-term measurements were performed with the catalyst in the continuous generation of $H_2$ over 8 days to generate ~11.2 mL of $H_2$ (Fig. S7, ESI†). Further, Cat-2 showed a significant amount of hydrogen evolution after the 1st cycle due to similar types of structural features to that of Cat-1 but with a lower nickel content (Fig. 1).

Furthermore, EPR spectroscopy has been applied as a very sensitive and local method for detecting selectively the formation of superparamagnetic $Ni^0$ nanoparticles (NP) which may be too

Published on 15 October 2015. Downloaded on 19/05/2017 11:54:47.

small or too few to be visualized by TEM.[32] The EPR spectrum of Cat-2 (Ni deposition in the dark) at 300 K showed no signal, suggesting that all nickel is dispersed as $Ni^{2+}$ species. After irradiation with visible light (in Cat-1) a broad EPR signal ($g$ = 2.23) could be observed, indicating the formation of ferromagnetic $Ni^0$ particles (Fig. S8, ESI†),[33] which illustrate the high sensitivity of EPR spectroscopy for the detection of $Ni^0$ cluster. By investigating the temperature dependence of the EPR signal intensity, an average $Ni^0$ particle diameter could be estimated using the Langevin equation (see ESI†).

Comparison of the experimental data of Cat-1 with the results for different particle diameters, suggests that the mean $Ni^0$ particle size in Cat-1 is around 3 nm (Fig. S9 and eqn (S1), ESI†). When Cat-1 is exposed to air during recovery, the $Ni^0$ signal strongly decreases, broadens and becomes more asymmetric. This might be an indication for the partial oxidation of the Ni NPs to $Ni^{2+}$ (Fig. S8, ESI†). As mentioned earlier, the main objective of this work is to determine the co-catalyst structure during the photocatalytic hydrogen evolution, *in situ* EPR spectroscopic studies were performed to prove the formation of the $Ni^0$ NPs under visible light irradiation. Cat-1 has been monitored by *in situ* EPR in a TEOA/$H_2O$ (1 : 9) solution under irradiation with visible light (>420 nm, Fig. 2). A continuous increase of the $Ni^0$ signal was detected, though, not all $Ni^{2+}$ species were reduced to $Ni^0$ at the same time (Scheme 1). This could be one of the reasons for the detection of a very small amount of $Ni^0$ in XPS after 48 h of irradiation.

Furthermore, EPR spectroscopy has been utilized to study charge separation processes in sg-CN as well as the impact of the co-catalyst on electron transfer. As reported previously, trapped conduction band electrons (CB-$e^-$) in sg-CN can be visualized by EPR during irradiation.[34] Charge separation efficiency can also be analyzed from EPR during irradiation (Fig. S10, black, ESI†). The latter corresponds to the photoactive CB-$e^-$ trapped at the surface. Furthermore, the recombination efficiency of these CB-$e^-$ with holes is indicated by a decrease of the EPR signal after irradiation (Fig. S10, red, ESI†). Highest charge separation as well as lowest recombination efficiency was observed for co-catalyst-free sg-CN. However, with the Ni-co-catalysts, in all samples, even less than half of the CB-$e^-$ concentration could be detected compared to 'free' sg-CN. This suggests that the CB-$e^-$ formed by light-induced charge separation within the support travels quickly to the co-catalyst, from which it is transferred to the protons to evolve dihydrogen.[34]

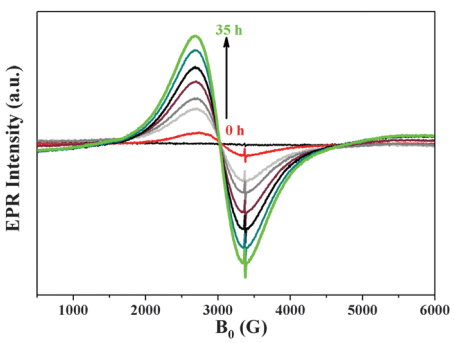


Fig. 2 *In situ* EPR studies of a suspension of Cat-1 in TEOA solution under continuous irradiation with visible light (>420 nm) with variation in time.

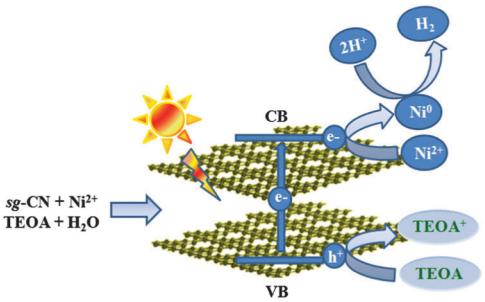


Scheme 1 Schematic representation of the charge separation in sg-CN and the formation of $Ni^0$ nanoparticles during photocatalytic hydrogen evolution under visible light irradiation.

Irradiation of sg-CN with visible light generates holes in the valence band and electrons in the conduction band (Scheme 1 and eqn (1)). Migration and separation of the charge was facilitated by the nickel. TEOA is able to quench the photogenerated holes in the valence band and acts as a sacrificial electron donor whereas the conduction band electrons reduce the protons to give dihydrogen. *In situ* reduction of $Ni^{2+}$ to $Ni^0$ *via* electron transfer from the conduction band (CB) can also occur which explains the formation of $Ni^0$ NPs (eqn (4)). Under photocatalytic conditions the reduction potential of carbon nitride conduction band (−1.3 V) is large enough to reduce $Ni^{2+}$ to $Ni^0$ (−0.26 V).[35,24b] The latter can act as a co-catalyst during proton reduction. Therefore, the actual catalyst system contains both $Ni^{2+}$ (XPS), and $Ni^0$ (EPR, XPS) species. The present system is significantly different from the $Ni^{2+}$–fluorescein system reported by Fu and co-workers where irradiation with visible light generated Ni NPs in the reaction medium.[24b] Transfer of the holes from the valence band of sg-CN to $Ni^{2+}$ can also occur to generate $Ni^{3+}$ as reported by Shangguan and co-workers in photodeposited $Ni_2O_3$–CdS.[36] A similar conclusion was drawn from NiOOH–$TiO_2$ systems, when a $Ni^{2+}$ salt was photodeposited by UV light on $TiO_2$ in the presence of a surfactant.[37] Furthermore, in this study, XPS shows that prolonged irradiation results in the movement of surface $Ni^0$ to the bulk, since only a low amount of nickel could be observed on the surface after a long reaction time. The formation of $Ni^0$ domains could be proved by *in situ* EPR spectroscopy. Elemental nickel is formed only under photocatalytic reaction conditions and is reoxidized quickly when exposed to air during isolation. Particles with higher contrast have been detected by HRTEM after recycling of Cat-1 after 8 days (Fig. 1b). The lattice spacing and the corresponding fast Fourier transform (FFT) indicates that the particles were oxidized to $Ni(OH)_2$. The nature of the $Ni^{2+}$ is expected to be similar to $Ni(TEOA)_2Cl_2$ as reported by Sun and co-workers.[23b]

$$\text{sg-CN} + h\nu \rightarrow e_{\text{sg-CN-CB}}^- + h_{\text{sg-CN-VB}}^+ \quad (1)$$

$$\text{TEOA} + h_{\text{sg-CN-VB}}^+ \rightarrow \text{TEOA}^+ \quad (2)$$

$$2H^+ + 2e_{\text{sg-CN-CB}}^- \rightarrow H_2 \quad (3)$$

$$Ni^{2+} + 2e_{\text{sg-CN-CB}}^- \rightarrow Ni^0 \quad (4)$$


This journal is © The Royal Society of Chemistry 2016

Published on 15 October 2015. Downloaded on 19/05/2017 11:54:47.

In conclusion, the nature of the active species in a noble metal-free nickel-containing sol–gel prepared mesoporous graphitic carbon nitride (sg-CN) system, for the photocatalytic hydrogen production in the presence of sacrificial agent, has been uncovered for the first time by *in situ* EPR spectroscopy. In addition, the formed catalytic species were also investigated by *ex situ* EPR, XPS, TEM, HRTEM. *In situ* EPR studies clearly proved that $Ni^{2+}$ has been reduced to $Ni^0$ NPs during the photocatalytic process and acts as a co-catalyst for the reduction of protons to dihydrogen. Quick transportation of the photogenerated electrons to the $Ni^0$ co-catalyst could also be observed by EPR spectroscopy after Ni loading on sg-CN. Photodeposition of $Ni^{2+}$ onto sg-CN leads to a photocatalytic system for the long-term photochemical proton reduction with activities comparable to other non-noble co-catalyst systems on sg-CN. Finally, the sg-CN system investigated here clearly provides insight into the co-catalyst structure during photochemical $H_2$ evolution and will help in the understanding of the electron–hole separation after the co-catalyst loading.

Financial support by the BMBF (L2H project) and the DFG (Cluster of Excellence UniCat) is gratefully acknowledged. D. H. thanks Dr Radnik for XPS measurements. We would also like to thank Dr Caren Göbel for the TEM measurements.

## Notes and references

1 H. B. Gray, *Nat. Chem.*, 2009, **1**, 1–7.
2 A. Indra, P. W. Menezes, M. Schwarze and M. Driess, *New J. Chem.*, 2014, **38**, 1942–1945.
3 J. Xing, W. Q. Fang, H. J. Zhao and H. G. Yang, *Chem. – Asian J.*, 2012, **7**, 642–657.
4 T. Hisatomi, J. Kubota and K. Domen, *Chem. Soc. Rev.*, 2014, **43**, 7520–7535.
5 J. Liu, J. Huang, D. Dontosova and M. Antonietti, *RSC Adv.*, 2013, **3**, 22988–22993.
6 K. Kailasam, J. D. Epping, A. Thomas, S. Losse and H. Junge, *Energy Environ. Sci.*, 2011, **4**, 4668–4674.
7 (*a*) T. Simon, N. Bouchonville, M. J. Berr, A. Vaneski, A. Adrović, D. Volbers, R. Wyrwich, M. Dö, A. S. Susha, A. L. Rogach, F. Jäckel, J. K. Stolarczyk and J. Feldmann, *Nat. Mater.*, 2014, **13**, 1013–1018; (*b*) J. Zhao, M. A. Holmes and F. E. Osterloh, *ACS Nano*, 2013, **7**, 4316–4325.
8 (*a*) X. Wang, K. Maeda, A. Thomas, K. Takanabe, G. Xin, J. M. Carlsson, K. Domen and M. Antonietti, *Nat. Mater.*, 2009, **8**, 76–80; (*b*) J. Zhang, Y. Chen and X. Wang, *Energy Environ. Sci.*, 2015, DOI: 10.1039/C5EE01895A; (*c*) Y. Zheng, L. Lin, B. Wang and X. Wang, *Angew. Chem., Int. Ed.*, 2015, **54**, 12868–12884.
9 D. Hollmann, M. Karnahl, S. Tschierlei, K. Kailasam, M. Schneider, J. Radnik, K. Grabow, U. Bentrup, H. Junge, M. Beller, S. Lochbrunner, A. Thomas and A. Brückner, *Chem. Mater.*, 2014, **26**, 1727–1733.
10 K. Maeda, K. Teramura, D. Lu, T. Takata, N. Saito, Y. Inoue and K. Domen, *Nature*, 2006, **440**, 295.
11 Z. Lin and X. Wang, *ChemSusChem*, 2014, **7**, 1547–1550.
12 G. Zhang, M. Zhang, X. Ye, X. Qiu, S. Lin and X. Wang, *Adv. Mater.*, 2014, **26**, 805–809.
13 M. Schwarze, D. Stellmach, M. Schroeder, K. Kailasam, R. Reske, A. Thomas and R. Schomäcker, *Phys. Chem. Chem. Phys.*, 2013, **15**, 3466–3472.
14 K. Kailasam, J. Schmidt, H. Bildirir, G. Zhang, S. Blechert, X. Wang and A. Thomas, *Macromol. Rapid Commun.*, 2013, **34**, 1008–1013.
15 Y. Hou, A. B. Laursen, J. Zhang, G. Zhang, Y. Zhu, X. Wang, S. Dahl and I. Chorkendorf, *Angew. Chem., Int. Ed.*, 2013, **52**, 3621–3625.
16 L. Ge, F. Zuo, J. Liu, Q. Ma, C. Wang, D. Sun, L. Bartels and P. Feng, *J. Phys. Chem. C*, 2012, **116**, 13708–13714.
17 F. Yang, V. Kuznietsov, M. Lublow, C. Merschjann, A. Steigert, J. Klaer, A. Thomas and T. Schedel-Niedrig, *J. Mater. Chem. A*, 2013, **1**, 6407–6415.
18 J. Hong, Y. Wang, Y. Wang, W. Zhang and R. Xu, *ChemSusChem*, 2013, **6**, 2263–2268.
19 J. Yu, S. Wang, B. Cheng, Z. Lin and F. Huang, *Catal. Sci. Technol.*, 2013, **3**, 1782–1789.
20 Y. Wang, R. Shi, J. Lin and Y. Zhu, *Energy Environ. Sci.*, 2011, **4**, 2922–2929.
21 X. Bai, R. Zong, C. Li, D. Liu, Y. Liu and Y. Zhu, *Appl. Catal., B*, 2014, **147**, 82–91.
22 S. Samanta, S. Martha and K. Parida, *ChemCatChem*, 2014, **6**, 1453–1462.
23 (*a*) S.-W. Cao, X.-F. Liu, Y.-P. Yuan, Z.-Y. Zhang, J. Fang, S. C. J. Loo, J. Barber, T. C. Sum and C. Xue, *Phys. Chem. Chem. Phys.*, 2013, **15**, 18363–18366; (*b*) J. Dong, M. Wang, X. Li, L. Chen, Y. He and L. Sun, *ChemSusChem*, 2012, **5**, 2133–2138.
24 (*a*) J.-J. Wang, Z.-J. Li, X.-B. Li, X.-B. Fan, Q.-Y. Meng, S. Yu, C.-B. Li, J.-X. Li, C.-H. Tung and L.-Z. Wu, *ChemSusChem*, 2014, **7**, 1468–1475; (*b*) C. Wang, S. Cao and W.-F. Fu, *Chem. Commun.*, 2013, **49**, 11251–11253.
25 B. C. M. Martindale, G. A. M. Hutton, C. A. Caputo and E. Reisner, *J. Am. Chem. Soc.*, 2015, **137**, 6018–6025.
26 (*a*) P. W. Menezes, A. Indra, O. Levy, K. Kailasam, V. Gutkin, J. Pfrommer and M. Driess, *Chem. Commun.*, 2015, **51**, 5005–5008; (*b*) A. Indra, P. W. Menezes and M. Driess, *ChemSusChem*, 2015, **8**, 776–785.
27 (*a*) A. Indra, P. W. Menezes, N. R. Sahraie, A. Bergmann, C. Das, M. Tallarida, D. Schmeißer, P. Strasser and M. Driess, *J. Am. Chem. Soc.*, 2014, **136**, 17530–17536; (*b*) A. Indra, P. W. Menezes, I. Zaharieva, E. Baktash, J. Pfrommer, M. Schwarze, H. Dau and M. Driess, *Angew. Chem., Int. Ed.*, 2013, **52**, 13206–13210.
28 (*a*) P. W. Menezes, A. Indra, P. Littlewood, M. Schwarze, C. Göbel, R. Schomäcker and M. Driess, *ChemSusChem*, 2017, **7**, 2202–2211; (*b*) P. W. Menezes, A. Indra, N. R. Sahraie, A. Bergmann, P. Strasser and M. Driess, *ChemSusChem*, 2015, **8**, 164–171; (*c*) P. W. Menezes, A. Indra, D. González-Flores, N. R. Sahraie, I. Zaharieva, M. Schwarze, P. Strasser, H. Dau and M. Driess, *ACS Catal.*, 2015, **5**, 2017–2027.
29 G. Zhang, G. Li and X. Wang, *ChemCatChem*, 2015, **7**, 2864–2870.
30 E. Ech-chamikh, A. Essafti, Y. Ijdiyaou and M. Azizan, *Sol. Energy Mater. Sol. Cells*, 2006, **90**, 1420–1423.
31 (*a*) S.-W. Cao, X.-F. Liu, Y.-P. Yuan, Z.-Y. Zhang, J. Fang, S. C. J. Loo, J. Barber, T. C. Sum and C. Xue, *Phys. Chem. Chem. Phys.*, 2013, **15**, 18363–18366; (*b*) J. Dong, M. Wang, X. Li, L. Chen, Y. He and L. Sun, *ChemSusChem*, 2012, **5**, 2133–2138.
32 (*a*) A. Brückner, U. Bentrup, H. Zanthoff and D. Maschmeyer, *J. Catal.*, 2009, **266**, 120–128; (*b*) F. Alonso, P. Riente, J. A. Sirvent and M. Yus, *Appl. Catal., A*, 2010, **378**, 42–51.
33 T. Isobe, R. A. Weeks and R. A. Zuhr, *Solid State Commun.*, 1998, **105**, 469–472.
34 J. B. Priebe, M. Karnahl, H. Junge, M. Beller, D. Hollmann and A. Brückner, *Angew. Chem., Int. Ed.*, 2013, **52**, 11420–11424.
35 S. Chu, Y. Wang, Y. Guo, J. Feng, C. Wang, W. Luo, X. Fan and Z. Zou, *ACS Catal.*, 2013, **3**, 912–919.
36 X. Chen, W. Chen, P. Lin, Y. Yang, H. Gao, J. Yuan and W. Shangguan, *Catal. Commun.*, 2013, **36**, 104–108.
37 L. Zhang, Y. Zhong, Z. He, J. Wang, J. Xu, J. Cai, N. Zhang, H. Zhou, H. Fan, H. Shao, J. Zhang and C. Cao, *J. Mater. Chem. A*, 2013, **1**, 4277–4285.